Magnetic excitations in the Zn-Mg-Tb icosahedral quasicrystal: An inelastic neutron scattering study

Taku J. Sato*
Neutron Science Laboratory, Institute for Solid State Physics, University of Tokyo, 106-1 Shirakata, Tokai, Ibaraki 319-1106, Japan and SORST, Japan Science and Technology Agency, Kawaguchi, Saitama 332-0012, Japan

Hiroyuki Takakura
Research Center for Molecular Thermodynamics, Graduate School of Science, Osaka University, Toyonaka, Osaka 560-0043, Japan and SORST, Japan Science and Technology Agency, Kawaguchi, Saitama 332-0012, Japan

An Pang Tsai
Institute of Multidisciplinary Research for Advanced Materials, Tohoku University, Sendai 980-8577, Japan and SORST, Japan Science and Technology Agency, Kawaguchi, Saitama 332-0012, Japan

Kaoru Shibata
Japan Atomic Energy Research Institute, Tokai, Ibaraki 319-1195, Japan
(Received 4 October 2005; published 10 February 2006)

Low-temperature spin dynamics in the face-centered-icosahedral Zn-Mg-Tb quasicrystal has been investigated by inelastic neutron scattering around its spin-glass-like freezing temperature ($T_f \simeq 5.8$ K). A single broad inelastic peak, centered at $\hbar\omega \simeq 2.5$ meV, was observed in the inelastic scattering spectrum at temperatures ranging from the base temperature up to ~20 K. The inelastic peak energy is $\boldsymbol{Q}$ independent, whereas the peak intensity shows weak $\boldsymbol{Q}$ dependence, which is qualitatively similar to that observed for the elastic diffuse scattering. The inelasticity of spin excitations is hardly seen in canonical spin glasses and thus is a distinct feature of the Zn-Mg-Tb quasicrystal. We argue, with an aide of numerical simulation, that this broad inelastic peak can be interpreted as localized collective fluctuations of short-range-ordered spins in a dodecahedral spin cluster. In a much lower-energy region ($\hbar\omega < 0.8$ meV), we observed a strong quasielastic signal, appearing only above T_f; its peak width decreases as the temperature is lowered and vanishes at T_f. It is thus evident that the quasielastic signal corresponds to a slow spin dynamics that freezes at the macroscopic freezing temperature. The coexistence of the inelastic peak and quasielastic signal suggests that the short-range order in the single cluster is robustly formed but is dynamic for $T_f < T < 20$ K. The macroscopic freezing at T_f is, thus, attributed to a random freezing of spin-cluster fluctuations.

DOI: 10.1103/PhysRevB.73.054417 PACS number(s): 75.50.Kj, 61.44.Br, 78.70.Nx

I. INTRODUCTION

Quasicrystals have distinct spatial symmetry characterized by highly ordered but nonperiodic (quasiperiodic) atomic structure, which differs from both periodic and random structures.[1,2] Ordering and excitations of quasiperiodically arranged magnetic moments (spins) are yet fundamental open problems, despite the intensive efforts continuously made since the discovery of the quasicrystal.[3]

Theoretically, the following two issues may be of current interest: quasiperiodic spin systems with frustrated spin-spin interactions and quasiperiodic quantum-spin systems. While it has been long known that unfrustrated quasiperiodic spin systems show trivial long-range order, recent Monte Carlo studies of frustrated quasiperiodic spin systems (spins on the Penrose lattice with dipolar interactions or on the Ammann-Beenker tiling with antiferromagnetic exchange-type interactions) show noncollinear complex spin order.[4,5] Knowledge of the unfrustrated quasiperiodic spin systems has also been elaborated on by investigating an effect of quantum fluctuations on the ground-state spin order and excitations. For example, an inhomogeneous ground state with hierarchical moment distribution was inferred for the antiferromagnetic quantum Heisenberg model on the two-dimensional bipartite quasiperiodic lattice.[6] Its excitation spectrum was shown to be also hierarchical with low-lying Goldstone modes.[7]

While theoretical study has been performed on various ideal quasiperiodic spin systems, experimental study is of course restricted to existing magnetic quasicrystals. The Zn-Mg-R (R=rare earth) icosahedral quasicrystals[8] are the most extensively studied magnetic quasicrystals because of the following experimental advantages. First, they have well-localized, mostly isotropic and sizable $4f$ magnetic moments ($\sim 10\mu_B$ for R=Tb).[9] Second, their atomic structure is relatively well known; highly ordered quasiperiodic structure is inferred in several structural investigations.[10–12] Single-grain availability is also an outstanding advantage of the Zn-Mg-R quasicrystals.[13–15] Magnetic studies of the Zn-Mg-R quasicrystals may be summarized as follows. In bulk magnetic susceptibility, the Zn-Mg-R quasicrystals exhibit irreversibility for field-cooled and zero-field-cooled runs below certain temperatures T_f [$T_f \sim 5.8$ K for R=Tb (Ref. 9)]. This is typical magnetization behavior of canonical spin glasses, and

 ©2006 The American Physical Society

thus in early studies the Zn-Mg-*R* quasicrystals were categorized in the spin-glass class.[16] The Weiss temperatures Θ are, however, antiferromagnetic and considerably larger than the corresponding freezing temperatures (for example $\Theta \simeq 26.3$ K for R=Tb), indicating a significant frustration effect reducing T_f. The relevance of the frustrations and antiferromagnetic interactions is also seen in static spin correlations observed in neutron diffraction studies; significant static short-range antiferromagnetic spin correlations have been detected in the Zn-Mg-Ho quasicrystals at the lowest temperature[17–20] with a correlation length of about 20 Å in full width at half maximum (FWHM). The short-range order is shown to have a six-dimensional modulation vector.[17] Such a significantly short-range-ordered frozen state has not been expected in the canonical spin glasses where completely random spin freezing is, instead, anticipated and suggests the existence of certain clusters of strongly coupled spins. Indeed, a simple dodecahedral spin cluster model was proposed as an initial model for the understanding of (three-dimensional) real-space spin configurations in the short-range-ordered region.[21] Recent study of magnetization relaxations also suggests that the spin freezing in Zn-Mg-Tb quasicrystal resembles that of superparamagnets to some extent, being a macroscopic indication of clustered spins at low temperatures.[22,23] In short, we now relatively well understand the antiferromagnetic short-range order, developed at the lowest temperature in the Zn-Mg-*R* magnetic quasicrystals.

While the short-range order is elucidated, the nature of spin freezing at T_f is still obscure. Questions such as, what is the relevant degree of freedom that freezes at T_f? or how can significant short-range order and typical spin-glass-like freezing be accommodated?, are intriguing but still open. To answer these questions, microscopic information on spin dynamics around T_f is apparently necessary. Neutron inelastic scattering is the most powerful tool to study the spin dynamics; however, only two preliminary powder-inelastic-scattering experiments have been performed to date.[24–26] These experiments provide scattering functions in very limited energy and Q ranges, and thus are apparently insufficient to deduce the details of the spin freezing. In this study, we have undertaken extensive neutron inelastic scattering experiments using both the powder and single grain of the face-centered icosahedral Zn-Mg-Tb quasicrystals. Three inelastic scattering spectrometers were combined to investigate magnetic excitations in the energy range of $0.05 < \hbar\omega < 80$ meV. With rich and detailed information obtained in the present experiments, we aim to reveal essential characteristics of spin dynamics, in particular the freezing phenomena observed macroscopically at T_f, in the Zn-Mg-Tb magnetic quasicrystal.

II. EXPERIMENTAL PROCEDURES

A polycrystalline sample (20 g) of nominal composition $Zn_{57}Mg_{34}Tb_9$ was prepared by melting constituent elements in an induction furnace using an Al_2O_3 crucible under an Ar gas atmosphere. Purities of the starting elements were 99.9999%, 99.99%, and 99.9% for Zn, Mg, and Tb, respectively. As-solidified alloys were subsequently annealed at T =773 K for 100 h to obtain a single-icosahedral-phased sample; high structural quality was confirmed by x-ray powder diffraction. A single grain of the Zn-Mg-Tb quasicrystal (about 1 cm^3) is grown by the Bridgman method.[13] The composition of melt was chosen to be $Zn_{40}Mg_{57.5}Tb_{2.5}$ (nominal), whereas the composition of the resulting single grain was determined as $Zn_{58}Mg_{33}Tb_9$ using energy-dispersive x-ray spectroscopy.

Powder neutron inelastic scattering experiments were performed using the inverted-geometry time-of-flight spectrometers LAM-D,[27] LAM-40,[28] and LAM-80ET,[29] all installed at KENS, KEK, Japan. Pyrolytic graphite (PG) 002 reflections were employed for analyzers to fix the final energy at E_f =4.59 meV for LAM-D and LAM-40, whereas mica 006 reflections were used at LAM-80ET with fixed final energy of E_f=1.91 meV. The energy resolution was estimated using a vanadium standard as $\Delta\hbar\omega \sim 480$ μeV (LAM-D), $\Delta\hbar\omega \sim 320$ μeV (LAM-40), or $\Delta\hbar\omega \sim 20$ μeV (LAM-80ET) (FWHM) at the elastic position. The powdered sample was loaded in a thin Al sample cell and inserted into a standard Orange cryostat. Background was carefully subtracted using proper combinations of empty-cell data and sample-shaped-Cd (absorber) data, whereas absorption correction was made using numerically calculated absorption factors. A polycrystalline sample of the Zn-Mg-Y quasicrystal was also measured as a nonmagnetic reference; nuclear inelastic scattering was confirmed to be negligible in the present Q, $\hbar\omega$, and T ranges.

Single-quasicrystal inelastic scattering experiments were performed at the LAM-40 spectrometer. The single-quasicrystalline sample was mounted at the bottom of the sample stick and inserted into the standard Orange cryostat; ω rotation was realized by rotating the sample stick. The raw data obtained were corrected in the same manner as the powder experiments.

Additional elastic scattering experiments were performed using the ISSP-GPTAS spectrometer installed at JRR-3M, JAERI, Japan. The spectrometer was operated in a double-axis mode with the PG 002 reflections used for the monochromator to select neutrons with E_i=14.61 meV. Higher-harmonic neutrons were eliminated by the PG filter. The collimations 40′-80′-40′ were used for most of the data acquisitions.

III. EXPERIMENTAL RESULTS

A. Overall features obtained using powder sample

Using the powder Zn-Mg-Tb sample, we first investigate overall features of the excitation spectrum at several temperatures ranging from 1.5 K to 50 K in a wide energy range up to 80 meV. Shown in Fig. 1 is the resulting scattering functions $S(Q,\hbar\omega)$ observed at 2θ=35° using the LAM-D spectrometer. It should be noted that they are results of constant-2θ scans, and thus Q is not fixed. ($Q \simeq 0.9$ Å^{-1} at the elastic position.) The inelastic spectrum at the lowest temperature (T=1.5 K $< T_f$) shows a peak around 2 meV. (A slight dip at 7 meV may be of spurious origin, since it could not be observed in the LAM-40 experiment with higher statistics, as shown later.) As the temperature is increased, the

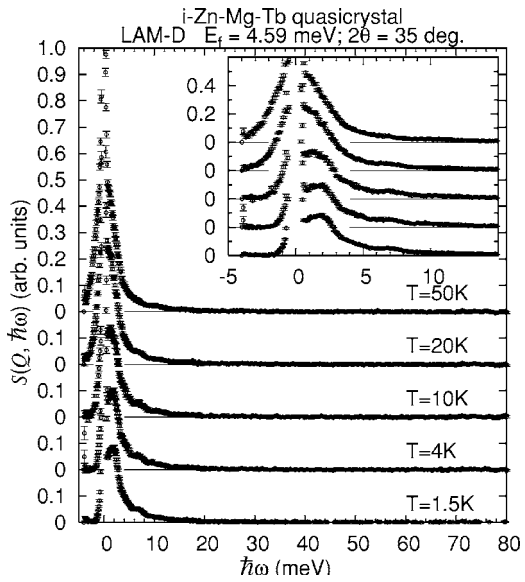

FIG. 1. Inelastic spectra in a wide energy range up to 80 meV observed at the LAM-D spectrometer. Results at several temperatures from 1.5 K to 50 K are shown. Inset: magnified plot for the low-energy region $-5<\hbar\omega<15$ meV.

peak is smeared by the quasielastic component; at $T=50$ K, the spectrum is dominated by a single broad quasielastic peak centered at $\hbar\omega=0$ meV. It should be noted here that the intensity above 20 meV is negligible. We thus conclude that magnetic scattering mainly appears in the low-energy region ($\hbar\omega<20$ meV) in the Zn-Mg-Tb quasicrystal.

To obtain detailed information in the low-energy region, we then performed powder inelastic scattering experiment using the LAM-40 spectrometer. Shown in Fig. 2(a) is the resulting scattering function $S(Q,\hbar\omega)$ measured for $8°<2\theta<116°$ with a 2θ step of 4°. The prominent inelastic peak is now seen at the energy transfer $\hbar\omega\sim2.5$ meV. The peak energy is a constant of Q, indicating a strongly localized origin of the corresponding excitation mode. The integrated intensity of the spectrum for $2<\hbar\omega<3$ meV is shown in Fig. 2(b) to visualize the Q dependence of the peak intensity. Also shown is the elastic magnetic-diffuse-scattering intensity obtained from the temperature difference $S(Q,\hbar\omega\sim0)|_{T=1.4\text{ K}}-S(Q,\hbar\omega\sim0)|_{T=100\text{ K}}$. The elastic intensity exhibits peaks at $Q\sim0.55$, 1.15, and 2.0 Å^{-1}, which perfectly coincide with the prior results.[18–20] On the other hand, the inelastic peak intensity shows a predominantly monotonous decrease for larger Q, which can be accounted for by the square of the Tb^{3+} magnetic form factor $|f(Q)|^2$ (dashed line). This confirms the magnetic origin of the inelastic peak. By looking carefully, however, one may find a weak intensity modulation in the Q dependence (solid line). It bears some resemblance to the Q dependence of the elastic intensity. This point will be further investigated using the single-quasicrystalline sample later.

As noted above, the Q dependence of $S(Q,\hbar\omega)$ is weak and predominantly monotonic. Thus, to increase the statistical accuracy, we sum up several $S(Q,\hbar\omega)$ observed simultaneously at different 2θ angles ($2\theta<68°$) and present it as the Q-integrated scattering function $S(\hbar\omega)$. Shown in Fig.

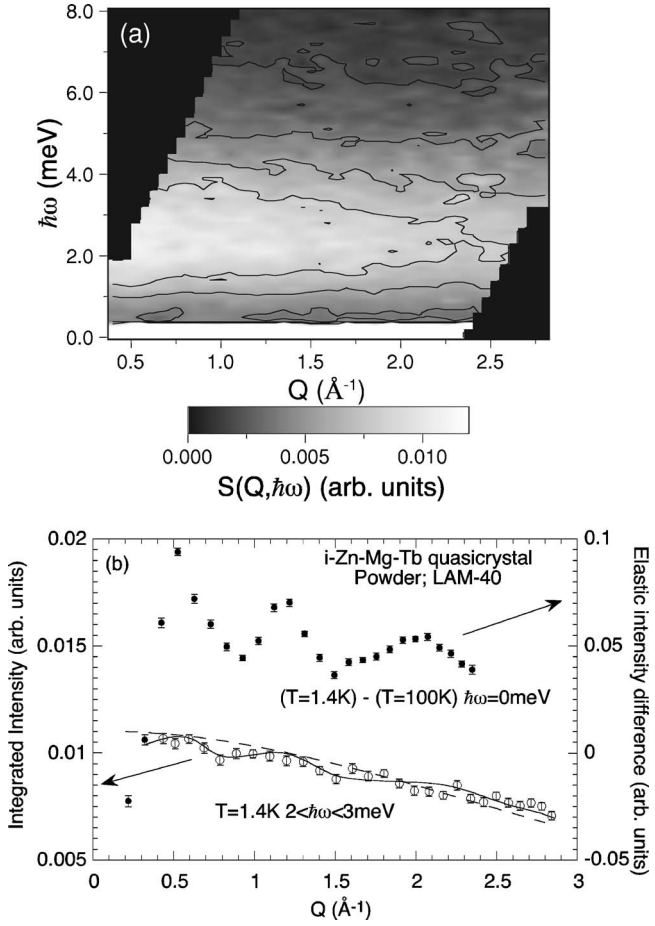

FIG. 2. (a) An inelastic scattering intensity map $S(Q,\hbar\omega)$ observed using the powder sample of the Zn-Mg-Tb quasicrystal at $T=1.4$ K. (b) Q dependence of the inelastic peak intensity (open circles) obtained by integrating the spectrum shown in (a) for $2<\hbar\omega<3$ meV. Solid circles stand for the elastic magnetic diffuse scattering intensity, obtained by the temperature difference $S(Q,\hbar\omega\sim0)|_{T=1.4\text{ K}}-S(Q,\hbar\omega\sim0)|_{T=100\text{ K}}$. The dashed line represents the square of the Tb^{3+} magnetic form factor, whereas the solid line is a guide for the eyes.

3(a) are resulting $S(\hbar\omega)$ at several temperatures from 1.4 K to 20 K. At the lowest temperature, the broad inelastic peak can be clearly seen at 2.5 meV. As the temperature is elevated, the inelastic scattering intensity gradually increases, in particular at lower energies. The inset of Fig. 3(a) shows the temperature dependence of the peak intensity integrated for $2<\hbar\omega<3$ meV. The intensity increase can be very prominently seen in this figure. Shown in Fig. 3(b) are temperature-factor-scaled spectra $S(\hbar\omega)/[1+n(\hbar\omega)]$ at the four temperatures $T=1.4$ K, 4 K, 8 K, and 12 K, where $n(\hbar\omega)=[\exp(\hbar\omega/k_BT)-1]^{-1}$ is the Bose temperature factor. All the scaled spectra coincide perfectly for the entire energy range below 12 K ($\sim2T_f$). The neutron scattering function is related to the imaginary part of the dynamic susceptibility as[30]

$$S(\hbar\omega)\propto[1+n(\hbar\omega)]\text{Im}\,\chi(\hbar\omega). \quad (1)$$

Thus, the scaling behavior indicates that Im $\chi(\hbar\omega)$ is independent of temperature below 12 K, or in other words, the

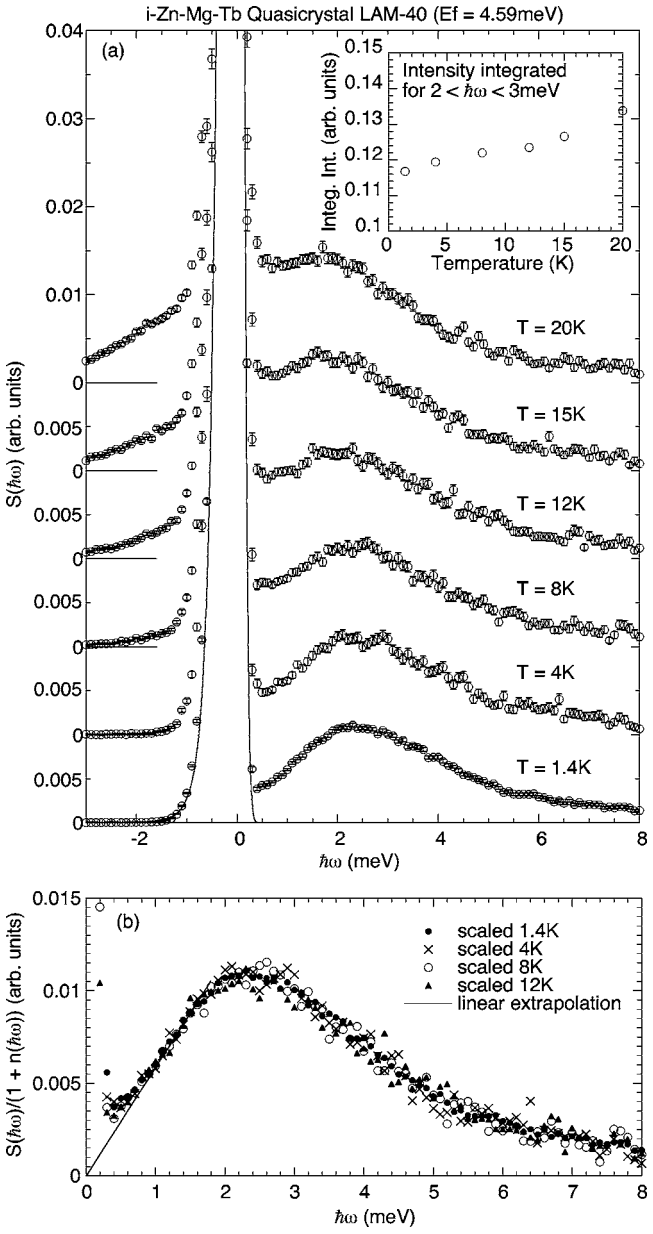

FIG. 3. (a) Q-integrated scattering function $S(\hbar\omega)$ at several temperatures; intensities observed at several angles covering $2\theta < 68°$ ($Q < 1.7$ Å^{-1} at the elastic position) are summed to increase statistics. The solid line stands for the vanadium standard spectrum as the instrumental resolution function. Inset: temperature dependence of the integrated intensity for $2 < \hbar\omega < 3$ meV. (b) Temperature-factor-scaled spectra $\mathrm{Im}\,\chi(\hbar\omega) \propto S(\hbar\omega)/[1+n(\hbar\omega)]$ for $T \leqslant 12$ K. The solid line stands for a linear extrapolation to $\hbar\omega \to 0$.

temperature dependence of the scattering intensity is solely given by the temperature factor $[1+n(\hbar\omega)]$.

At much higher temperatures (15 K and 20 K), there appears an additional quasielastic intensity around $\hbar\omega=0$ and the broad inelastic peak becomes relatively unclear. Concomitantly, temperature-factor scaling becomes unsatisfactory. Details of this quasielastic component will be further investigated with a much higher-energy resolution in the later sections.

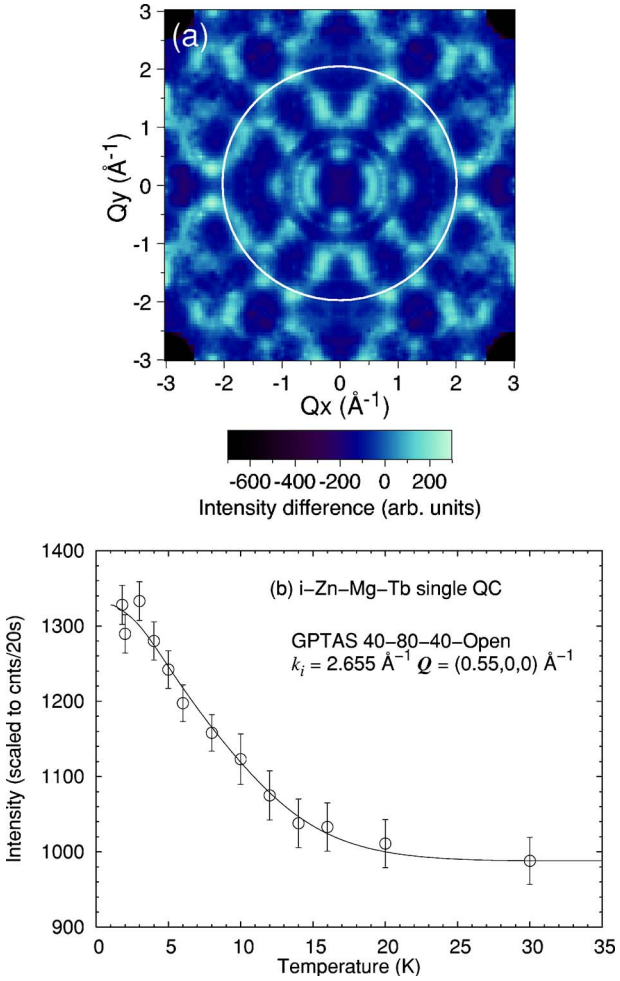

FIG. 4. (a) (Color online) Magnetic diffuse scattering intensity map in the 2F plane at $T=1.4$ K. The temperature difference $S(\boldsymbol{Q})|_{T=1.4\ \mathrm{K}} - S(\boldsymbol{Q})|_{T=30\ \mathrm{K}}$ was used to deduce the magnetic component. The white circle represents the $\boldsymbol{Q}$ region where the inelastic intensity is shown in Fig. 5. Data are corrected for the square of the Tb^{3+} magnetic form factor. (b) Temperature dependence of the elastic diffuse scattering peak observed at $\boldsymbol{Q}=(0.55,0,0)$ Å^{-1}. Raw data, measured with several different acquisition times, are scaled to counts per 20 s.

B. Single-quasicrystal results

Next, we investigate $\boldsymbol{Q}$-directional dependence of the scattering function using the single-quasicrystalline sample. Before going into inelastic experiment results, we just briefly reexamine elastic diffuse scattering in the present R=Tb system, since earlier experiments were performed only on the Ho system.[17,20] Shown in Fig. 4(a) is a magnetic diffuse scattering map in the twofold (2F) plane of the Zn-Mg-Tb quasicrystal, obtained in the present study in the same manner as Zn-Mg-Ho.[17,20] Strong magnetic diffuse scattering can be seen in the map, confirming the development of static short-range-spin correlations. The correlation length is estimated as about 20 Å (FWHM). The intensity map is qualitatively identical with that observed in Zn-Mg-Ho, indicating that the static short-range order is independent of rare-earth elements. Shown in Fig. 4(b) is the temperature dependence

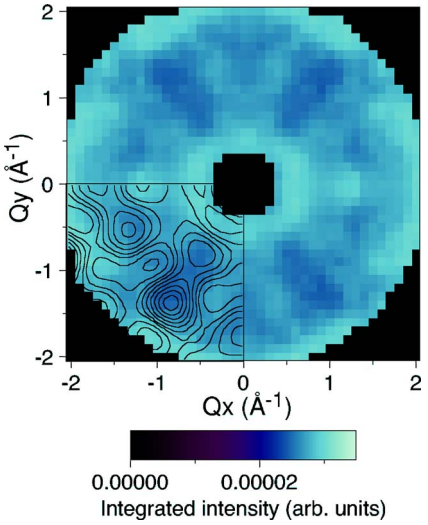

FIG. 5. (Color online) Inelastic scattering intensity map in the 2F plane, obtained by integrating spectra at $T=1.4$ K for $1<\hbar\omega<4$ meV. The superimposed contour map stands for the magnetic diffuse scattering intensity shown in Fig. 4(a) for comparison. Data are corrected for the square of the Tb^{3+} magnetic form factor.

of the diffuse peak intensity. As can be seen in the figure, the magnetic diffuse peak evolves below $T\simeq 20$ K, which is considerably higher than the macroscopic freezing temperature. Similar behavior was observed in the Zn-Mg-Ho quasicrystal.[17]

Using this Zn-Mg-Tb single-quasicrystalline sample, we measured the inelastic scattering function $S(\boldsymbol{Q},\hbar\omega)$ in half of the 2F plane for $-3<\hbar\omega<8$ meV. Observation was made with a 2θ step of 5.3° and an ω step of 6°, corresponding to a $\boldsymbol{Q}$ step of $\Delta Q\sim 0.1$ Å^{-1} at $Q\sim 1$ Å^{-1} and $\hbar\omega=0$ meV. The resulting inelastic spectra exhibit the broad inelastic peak, as observed in the powder experiment, at all $\boldsymbol{Q}$ positions with constant excitation energy; no energy dispersion was detected in this single-quasicrystal experiment within the present experimental accuracy. In contrast, its intensity shows detectable $\boldsymbol{Q}$ dependence, and thus, we here focus on the $\boldsymbol{Q}$ dependence of the inelastic scattering intensity. Shown in Fig. 5 is the inelastic scattering intensity map in the 2F plane observed at the lowest temperature. To obtain the figure, first the raw spectrum is integrated for $1<\hbar\omega<4$ meV at each $\boldsymbol{Q}$. Then, the obtained integrated-intensity map is folded in one symmetrically independent region to gain higher statistics and unfolded to the entire 2F plane to increase visibility. The $\boldsymbol{Q}$ region for this inelastic experiment was restricted to $Q<2$ Å^{-1} because of the decreasing intensity at higher Q due to the magnetic form factor. Although the inelastic intensity map has a very smoothed contrast, it obviously exhibits noticeable nonspherical $\boldsymbol{Q}$ dependence, which is qualitatively similar to the elastic one [Fig. 4(a)]. This similarity becomes evident by superimposing a contour line plot of the elastic diffuse scattering on the inelastic map (see contour lines in Fig. 5).

C. Quasielastic energy region

Spin excitations are investigated in a much lower-energy region $\hbar\omega<0.8$ meV using the LAM-80ET spectrometer.

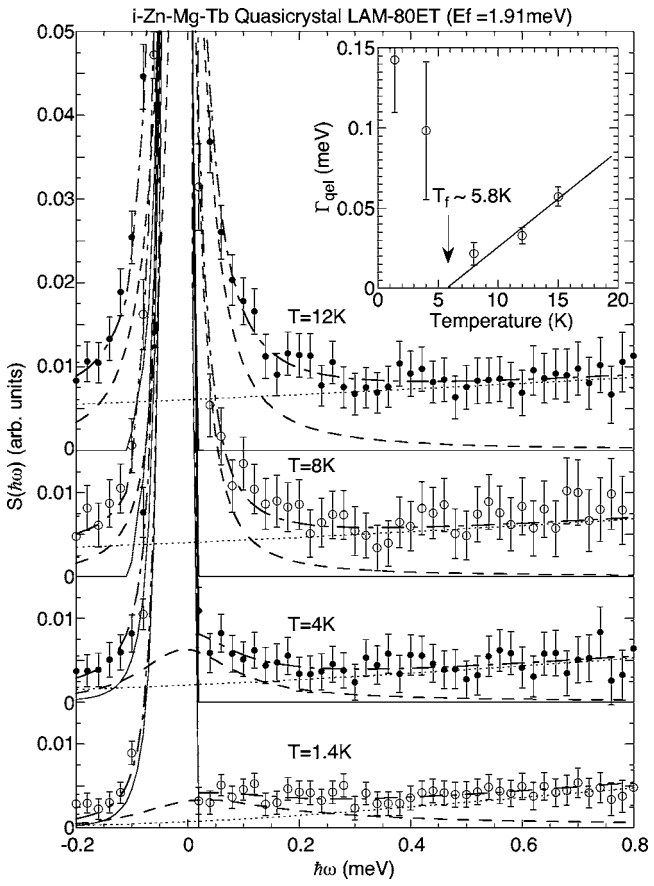

FIG. 6. Dynamic scattering function $S(\hbar\omega)$ observed using LAM-80ET. Intensities from eight counters covering $2\theta<115°$ ($Q<1.7$ Å^{-1} at the elastic position) are averaged and normalized to the LAM-40 results using the overlapping energy region. The dash-dotted lines represent resolution-convoluted fitting results to the trial scattering function, Eq. (2), whereas the solid, dotted, and dashed lines stand for each term in the function—i.e., elastic, linear-extrapolation, or quasielastic terms. Inset: temperature dependence of the quasielastic peak width $\Gamma_{\rm qel}$, obtained by resolution-convoluted fitting. See text for details.

Again, the powder sample was used because a large sample volume is necessary for this very-high-energy-resolution experiment. Shown in Fig. 6 are the resulting Q-integrated spectrum observed at $T=1.4$, 4, 8, and 12 K. Also shown by the dotted lines is a linear extrapolation of the high-energy data ($0.5<\hbar\omega<2.0$ meV) shown in Fig. 3(b). One may find excess scattering intensity even at the lowest temperature $T=1.4$ K, which adds to the linear extrapolation. To parametrize the spectrum, we assume the following scattering function in this lower-energy region:

$$S(\hbar\omega)=C_{\rm elastic}\delta(\hbar\omega)+C_{\rm linear}[1+n(\hbar\omega)]\hbar\omega + C_{\rm qel}[1+n(\hbar\omega)]\frac{\hbar\omega\Gamma_{\rm qel}}{\Gamma_{\rm qel}^2+(\hbar\omega)^2}, \quad (2)$$

where the first, second, and third terms represent the elastic, linear-extrapolation, and quasielastic Lorentzian-type functions. Instrumental-resolution-convoluted fitting was performed using the above function; during the fitting proce-

dure, C_{linear} was fixed to the values determined from the higher-energy LAM-40 data. Solid, dotted, dashed, and dash-dotted lines in Fig. 6 represent the elastic, linear-extrapolation, quasielastic, and total scattering functions. As can be seen from the figure, the excess signal can be well fitted to the Lorentzian-type quasielastic function with $\Gamma_{\text{qel}}=0.14(3)$ meV at 1.4 K. The Lorentzian-type scattering function corresponds to an exponential decay of spin fluctuations, and thus this broad quasielastic scattering suggests the existence of a rather fast exponential relaxation even at the lowest temperature in the Zn-Mg-Tb quasicrystal. The relaxation time is estimated as $\tau=\hbar/\Gamma_{\text{qel}}\sim 4\times 10^{-12}$ s. As temperature is increased to $T=4$ K, the quasielastic peak width becomes slightly narrower as $\Gamma_{\text{qel}}\sim 0.10(4)$ meV. The temperature dependence of Γ_{qel} is summarized in the inset of Fig. 6. The origin of this fast relaxation is not clear at the present moment; we may suggest that in view of its weak intensity there may be a small number of uncorrelated fast-fluctuating spins in the quasicrystalline structure.

On crossing the freezing temperature T_{f}, there abruptly appears a much narrower and stronger quasielastic peak as seen in the $T=8$ and 12 K data in Fig. 6. This peak clearly indicates the existence of a slower relaxational mode above T_{f} and corresponds to the low-energy quasielastic intensity detected in the LAM-40 experiments [Fig. 3(a)]. The spectra above T_{f} are similarly fitted to the trial function, Eq. (2), and the resulting Γ_{qel} is also plotted in the inset of Fig. 6. It is clear from the figure that the width Γ_{qel} is temperature dependent for $T>T_{\text{f}}$; it sharpens as the temperature is lowered, and its width vanishes at T_{f}. This confirms that the slow relaxational dynamics detected in this temperature range is indeed responsible for the spin freezing observed in the macroscopic measurements.

IV. DISCUSSION

In canonical spin glasses, the low-energy spin dynamics below T_{f} is governed by relaxational processes with widely distributed characteristic time scales.[31,32] Consequently, the spin excitation spectrum is dominated by quasielastic scattering centered at $\hbar\omega=0$.[33] In striking contrast to the above standard description of spin dynamics in canonical spin glasses, the present the experiments undoubtedly show the existence of an inelastic peak in the Zn-Mg-Tb quasicrystal. To the best of our knowledge, the inelasticity of spin excitations cannot be seen in any kind of spin glasses, and thus is an essential feature distinguishing the spin-glass-like phase in quasicrystals from canonical spin glasses. Here, we will first discuss the origin of the inelastic excitation peak and then argue the nature of the freezing phenomena in this magnetic quasicrystal.

A. Origin of the inelastic peak: A dodecahedral spin cluster model

In rare-earth magnetic systems, transitions between crystalline electric field (CEF) splitting levels are the usual origin of localized inelastic excitations. However, the CEF transition intensity decreases at high temperatures, since the intensity is dominated by population of an initial state, given by the Boltzmann factor.[30] Thus, the observed increase of the inelastic peak intensity evidently excludes the CEF origin. Instead, the temperature-factor $[1+n(\hbar\omega)]$ scaling suggests that the inelastic peak is attributed to certain collective harmonic dynamics. The similarity of the $\boldsymbol{Q}$ dependence between the elastic and inelastic scattering further suggests that both scatterings share a common spin structure factor. Hence, the broad inelastic peak may most likely be attributed to the collective harmonic fluctuations of spins around their statically short-range-ordered directions. In our previous work,[21] we have proposed a dodecahedral spin cluster model as an initial model to understand the static short-range order. The dodecahedral cluster is the most frequently appearing cluster in the recently proposed structure model[10,11] with its diameter ($\sim$15 Å) comparable to the length scale of the short-range order. Furthermore, minimum-energy spin configurations of the dodecahedral spin cluster reproduce the observed elastic diffuse scattering patterns quite satisfactorily, indicating that the spin configurations in the short-range-ordered region in Zn-Mg-Tb are indeed given by the minimum-energy configurations of the dodecahedral cluster model.[21] Here, we will show that the presently observed broad inelastic peak can be also well reproduced using the same model by calculating its dynamic susceptibility at the lowest temperature.

The model Hamiltonian we assume here is the same as that in the previous work:[21]

$$\mathcal{H}=-\sum_{\langle \text{NNN}\rangle} J_{ij}\hat{\boldsymbol{J}}_i\cdot\hat{\boldsymbol{J}}_j, \tag{3}$$

where i (or j) stands for one of 20 vertex sites of the single dodecahedron with an edge length of 5.4 Å. $\hat{\boldsymbol{J}}_i$ ($\hat{\boldsymbol{J}}_j$) stands for an isotropic total angular momentum operator for Tb^{3+} at the ith (jth) site, and J_{ij} are exchange interaction parameters. $\langle$NNN$\rangle$ indicates that the summation is taken only for next-nearest-neighbor pairs with 8.8-Å separations; the next-nearest-neighbor interactions J_2 were found to be relevant antiferromagnetic interactions in the previous work. See Fig. 7 for the graphical representation of a single dodecahedral spin cluster.

Classical ground-state spin configurations were obtained by numerically minimizing Eq. (3); details of the minimizing procedure are given in Appendix A. Then, the dynamic susceptibility $\chi^{\text{RPA}}(\boldsymbol{Q},\hbar\omega)$ at the lowest temperature, defined as the response of spins in the classical ground states to an oscillating external magnetic field, was calculated within the random-phase approximation (RPA).[34] Details of the calculations are given in Appendix B, and here we only note that the present RPA calculation includes intersite interactions to leading order and thus gives collective linear-spin-wave-like excitations in the resulting dynamic susceptibility.

For the numerical RPA calculations, values of the second-nearest-neighbor interactions J_2 and width of single-site levels Γ_{s} are necessary since they determine the peak energy and width of collective inelastic modes. After trying several choices of the parameters, we found that the observed inelastic spectrum [shown in Fig. 3(b)] is reasonably reproduced

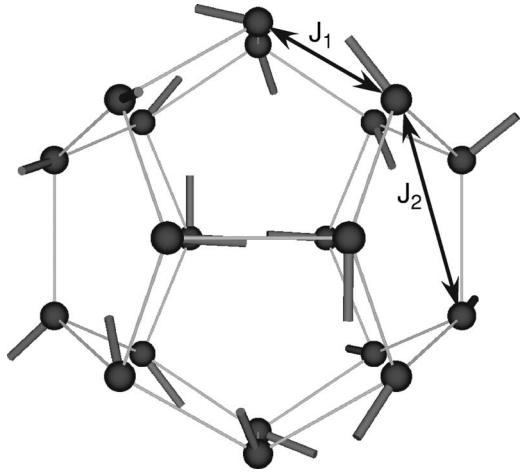

FIG. 7. Dodecahedral spin cluster model. A typical ground-state spin configuration is shown by the thick solid lines. The nearest-neighbor (J_1) and next-nearest-neighbor (J_2) interactions are also indicated by arrows.

with $J_2=-0.14$ meV and $\Gamma_s=1.8$ meV. The $\boldsymbol{Q}$-averaged dynamic susceptibility Im $\chi^{\mathrm{RPA}}(\hbar\omega)$ calculated with the above parameters is shown in Fig. 8(a). Comparing to the corresponding experimental result, one can find a quite satisfactory agreement. The $\hbar\omega$-integrated scattering function is estimated as

$$S_{\mathrm{inel}}^{\mathrm{RPA}}(\boldsymbol{Q}) = \int_{1\ \mathrm{meV}}^{4\ \mathrm{meV}} \mathrm{d}(\hbar\omega)[1+n(\hbar\omega)]\mathrm{Im}\ \chi^{\mathrm{RPA}}(\boldsymbol{Q},\hbar\omega). \tag{4}$$

The resulting $S_{\mathrm{inel}}^{\mathrm{RPA}}(\boldsymbol{Q})$ is shown in Fig. 8(b), which should be compared to the observed intensity map, Fig. 5. Noticeable coincidence can be readily seen, confirming the validity of the dodecahedral spin cluster model for describing not only elastic but also inelastic scattering in the Zn-Mg-Tb quasicrystal. This further confirms that the collective spin fluctuations of the short-range-ordered spins are responsible for the observed broad inelastic peak, as we expected from the $\boldsymbol{Q}$ and temperature dependence of the peak. It may be noteworthy, however, that in the quasicrystalline structure, the dodecahedral spin clusters are connected to each other by sharing their edges, forming a quasiperiodic network; there is no reason for the clusters to be treated independently, at least from a geometrical point of view. It is, thus, unclear why the collective fluctuations do not propagate to adjacent clusters. This quite intriguing problem is, though, left for further study.

B. Spin freezing

The diffuse scattering intensity, shown in Fig. 4(b), is finite even above T_f. Concomitantly, as shown in Fig. 3(a), the broad inelastic peak survives up to ~20 K. These results indicate that short-range order in the dodecahedral spin cluster is still formed for $T_f<T<20$ K. On the other hand, the low-energy experiments conducted at LAM-80ET (Fig. 6) reveal that the strong quasielastic signal abruptly appears at

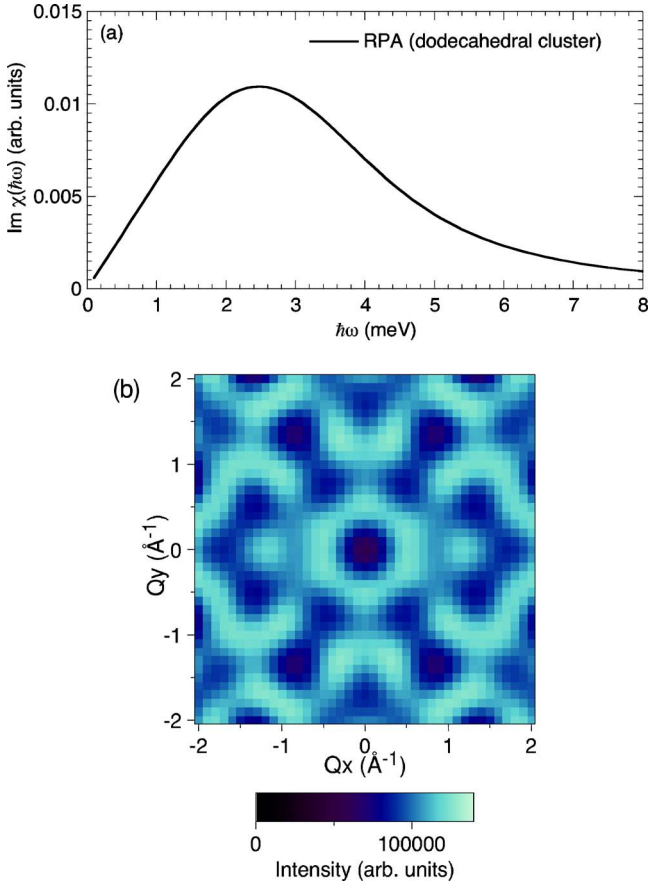

FIG. 8. (Color online) (a) Imaginary part of the calculated Q-integrated dynamic susceptibility Im $\chi^{\mathrm{RPA}}(\hbar\omega)$. (b) Calculated inelastic scattering intensity map in the 2F plane. Intensities for all the inelastic excitations in $1<\hbar\omega<4$ meV are integrated to obtain this $\hbar\omega$-integrated intensity map, as was done for obtaining the experimental map shown in Fig. 5.

T_f on increasing the temperature. Hence, the spins start to exhibit slow relaxational dynamics above T_f. Since the intracluster coherence is robustly maintained, this slow dynamics may most likely correspond to the motion of entire short-range-ordered spins in the dodecahedral cluster. We hence suggest that the degree of freedom that freezes at T_f is not a motion of individual spins, but is the motion of entire cluster spins.

As the temperature is further increased, the quasielastic peak width becomes larger and larger (see inset of Fig. 6), indicating that the corresponding cluster motion becomes considerably fast. When the time scale of the entire cluster motion becomes comparable to that of the intracluster collective fluctuations, the collective fluctuations can no longer be well defined. This may be the reason for the smearing inelastic peak above $T>20$ K. Hence, in the magnetic quasicrystal, there are at least two characteristic temperatures; at $T\sim 20$ K the formation of short-range-ordered spin clusters begins, but the clusters are still independently fluctuating, and by further decreasing the temperature the motion of the clusters freezes randomly at T_f. This microscopic description of spin freezing in the Zn-Mg-Tb quasicrystal is conceptually different from that in canonical spin glasses, where the

motion of individual spins freezes randomly at T_f. Therefore, a key to understanding the freezing behavior in the magnetic quasicrystal is the formation of dynamical short-range order well above the macroscopic freezing temperature T_f.

The existence of spin clusters might suggest a similarity to superparamagnets.[35] However, in the superparamagnets, the degree of freedom that freezes at the blocking temperature is the total magnetic moment of the cluster; since the spins in a cluster are coupled ferromagnetically in superparamagnets, the anisotropy energy for the total moment becomes comparable to the thermal excitation energy, resulting in the blocking of the spin motion at a certain blocking temperature. In the present Zn-Mg-Tb quasicrystal, significant single-site anisotropy is unlikely in view of the absence of CEF levels, and thus the simple blocking phenomena may not occur. The difference can be also seen in the freezing degree of freedom; since the spins are antiferromagnetically coupled in the dodecahedral clusters, the total moment is always zero and thus cannot be the freezing degree of freedom. Instead, continuous degeneracy of the ground state, originating from the high symmetry and geometrical frustration of the dodecahedral cluster, provides a way for entire cluster spins to fluctuate coherently without costing energy. This new degree of freedom may likely be responsible for the freezing. Hence, we suggest that even though the cluster formation is relevant, the spin freezing in the magnetic quasicrystal is different also from the blocking phenomena in the superparamagnets. In view of the absence of significant anisotropy, we rather suggest that the freezing may likely be cooperative.

C. Similarity to the topological glasses

Finally, we suggest a possible close relation to the so-called boson peak in topological glasses.[36,37] The boson peak is a broad inelastic excitation peak universally observed in vibrational spectra of the topological glasses at a Q-independent excitation energy of a few meV. Its intensity shows a Q dependence similar to the static structure factor (i.e., elastic scattering intensity), whereas its temperature dependence is given by the Bose temperature factor. The boson peak is believed to be related to collective atomic vibrations in a small structural unit responsible for the static structure factor $S(Q)$; an example of such a unit is a cluster of five tetrahedra in vitreous silica. [38] These characteristics are surprisingly similar to those of the presently observed inelastic peak, and thus at least phenomenologically, we may regard the inelastic peak as a spin analogy of the boson peak.

V. CONCLUSIONS

Our inelastic neutron scattering experiments in the wide energy range reveal two significant features of the spin excitation spectrum in the Zn-Mg-Tb quasicrystal at low temperatures. One is the broad inelastic peak at 2.5 meV, which is attributed to the collective harmonic fluctuations of the short-range-ordered spins in the dodecahedral spin cluster. The other is the quasielastic signal appearing in the higher vicinity of T_f, which is related to the motion of entire cluster spins. We suggest that the degree of freedom that freezes at the macroscopic freezing temperature T_f is the motion of entire cluster spins, but not individual ones; the freezing is thus very different from the canonical spin glasses or superparamagnets. Finally, we suggest a possible close relation between the presently observed magnetic excitation peak and the boson peak in the topological glasses.

ACKNOWLEDGMENTS

The present authors thank Dr. E. Abe, Dr. I. R. Fisher, Dr. I. Tsukushi, Dr. Y. Kawakita, Dr. H. Kadowaki, Dr. K. Kamazawa, Dr. S.-H. Lee, and Dr. J. W. Lynn for valuable suggestions and comments. This work was partly supported by a Grant-in-Aid for Encouragement of Young Scientists (B) (No. 16760537) and by a Grant-in-Aid for Creative Scientific Research (No. 16GS0417) from the Ministry of Education, Culture, Sports, Science and Technology of Japan.

APPENDIX A: MINIMUM-ENERGY SPIN CONFIGURATIONS OF THE DODECAHEDRAL SPIN CLUSTER MODEL

In this appendix, the determination of ground-state spin configurations will be described, which is supplemental to our previous work.[21]

Since the total angular moment of Tb^{3+} is quite as large as $J=6$, we may approximate it as classical vector spins. The classical energy is then given by replacing the quantum-mechanical operators $\hat{\boldsymbol{J}}$ in Eq. (3) to the classical vectors $\boldsymbol{J}$ as

$$E_{\mathrm{cl}} = -\sum_{\langle \mathrm{NNN} \rangle} J_{ij} \boldsymbol{J}_i \cdot \boldsymbol{J}_j. \tag{A1}$$

The summation is taken only for the next-nearest-neighbor pairs $\langle$NNN$\rangle$. (The next-nearest-neighbor interaction parameter is denoted by J_2.) Ground-state spin configurations $\{\boldsymbol{J}_i^{\mathrm{gs}}\}$ of the dodecahedral spin cluster model can be obtained by minimizing E_{cl}; for the numerical minimization, we used the UNCMIN code, implementing a quasi-Newton algorithm with line search.[39] The minimization was repeated for about 16 000 times with random initial spin configurations. Shown in Fig. 9 is the distribution of minimized energies. The minimum energy was found to be $E_{\mathrm{cl}}/(|J_2|J^2) \simeq -29.18$, whereas about 40% of the minimization trials fall into local minima with significantly higher energies. We thus discard spin configurations with $E_{\mathrm{cl}}/(|J_2|J^2) > -29.15$ and assume that configurations with lower energies are ground-state (minimum-energy) configurations.

We found that the ground-state spin configurations are quite complex and noncollinear, as typically shown in Fig. 7. The ground state is highly degenerated, in addition to a trivial Heisenberg rotational invariance; even with fixing one spin to the z axis, other spins have rotational degrees of freedom in the xy plane without costing extra energy. This may be related to the near-spherical symmetry of the dodecahedral cluster model. In addition, we found other discrete degeneracies corresponding to quantized relative angles between spins in different pentagonal layers, which are related to the geometrical frustration of this dodecahedral spin clus-

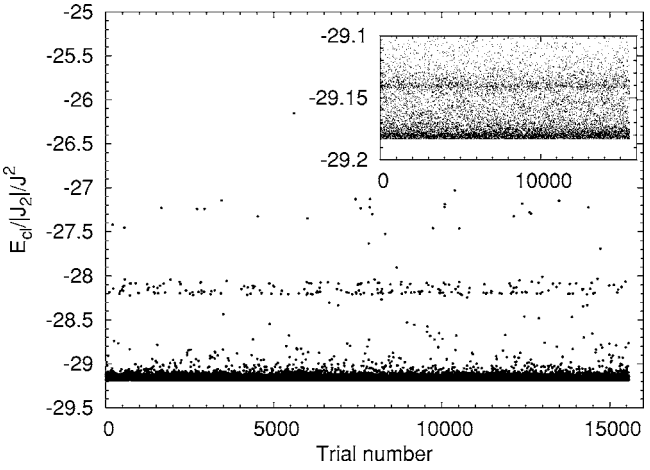

FIG. 9. Distribution of minimized classical energies of the dodecahedral spin cluster.

ter model. Despite the fact that the dodecahedral spin cluster is seemingly intriguing for further theoretical study, we will not pursue this problem since it is out of the scope of the present study. Here, we only note that the observed freezing behavior may be due to the high degeneracy, since in such a degenerated system very weak random perturbations, inevitable in real quasicrystals, may stabilize locally very different spin configurations. A similar situation may be seen in many geometrically frustrated magnets, exemplified by the pyrochlore antiferromagnet $Tb_2Mo_2O_7$.[40]

APPENDIX B: RPA CALCULATION OF THE DYNAMIC SUSCEPTIBILITY

To explore the spin dynamics of the dodecahedral spin cluster model at the lowest temperature, we calculate the dynamic susceptibility of the system within the random phase approximation. At the lowest temperature, it may be a good assumption that the magnetic moments are nearly saturated along their classical ground-state directions—i.e., $\langle \hat{\boldsymbol{J}}_i \rangle \simeq \boldsymbol{J}_i^{\text{g.s.}}$. For such a case, intersite interactions provide perturbations to single-site susceptibility determined by the local mean field in the RPA formalism, resulting in linear-spin-wave-like collective fluctuations around the saturation directions in the wave-vector-dependent dynamic susceptibility. The technical details and physical background of the RPA may be found in the textbook given in Ref. 34; we only provide specifics to the noncollinearity of the present dodecahedral model in this appendix.

In the RPA, the site-dependent dynamic susceptibility tensor $\bar{\bar{\chi}}_{ij}(\hbar\omega)$ is determined by the following self-consistent equations:[34]

$$\bar{\bar{\chi}}_{ij}(\hbar\omega) - \frac{1}{2}\bar{\bar{\chi}}_i^0(\hbar\omega)\sum_{j'} J_{ij'}\bar{\bar{\chi}}_{j'j}(\hbar\omega) = \bar{\bar{\chi}}_i^0(\hbar\omega)\delta_{ij}, \quad \text{(B1)}$$

where $\bar{\bar{\chi}}_i^0(\hbar\omega)$ is a single-site susceptibility tensor at the ith site, which is determined by the mean-field Hamiltonian

$$\mathcal{H}_i^{\text{MF}} = -\left(\hat{\boldsymbol{J}}_i - \frac{1}{2}\langle \hat{\boldsymbol{J}}_i \rangle\right) \cdot \left(\sum_j J_{ij}\langle \hat{\boldsymbol{J}}_j \rangle\right). \quad \text{(B2)}$$

Since the ground-state spin configurations of the dodecahedral cluster model are noncollinear, we now introduce site-dependent local coordinates spanned by three orthogonal column vectors $\boldsymbol{a}_i$, $\boldsymbol{b}_i$, and $\boldsymbol{n}_i$, where $\boldsymbol{n}_i$ is taken as $\boldsymbol{n}_i \| \langle \hat{\boldsymbol{J}}_i \rangle$. The spin operator $\hat{\boldsymbol{J}}_i^{xyz}$ in xyz coordinates is related to $\hat{\boldsymbol{J}}_i^{abn}$ defined in abn coordinates as

$$\hat{\boldsymbol{J}}_i^{xyz} = \begin{pmatrix} \hat{J}_i^x \\ \hat{J}_i^y \\ \hat{J}_i^z \end{pmatrix} = R_i \begin{pmatrix} \hat{J}_i^a \\ \hat{J}_i^b \\ \hat{J}_i^n \end{pmatrix} = R_i \hat{\boldsymbol{J}}_i^{abn}, \quad \text{(B3)}$$

where R_i is a 3×3 matrix defined as $R_i=(\boldsymbol{a}_i,\boldsymbol{b}_i,\boldsymbol{n}_i)$. In these local coordinates the mean-field Hamiltonian becomes site independent and so is $\bar{\bar{\chi}}_i^0(\hbar\omega)$. The site-independent $\bar{\bar{\chi}}_i^0(\hbar\omega)$ for $\hbar\omega \neq 0$ is easily obtained as[34]

$$\chi_i^{0aa}(\hbar\omega) = \chi_i^{0bb}(\hbar\omega) = \frac{\Delta\langle \hat{J}^n \rangle}{\Delta^2 - (\hbar\omega)^2}, \quad \text{(B4)}$$

$$\chi_i^{0ab}(\hbar\omega) = -\chi_i^{0ba}(\hbar\omega) = \frac{i\hbar\omega\langle \hat{J}^n \rangle}{\Delta^2 - (\hbar\omega)^2}, \quad \text{(B5)}$$

$$\chi_i^{0cc}(\hbar\omega) = 0, \quad \text{(B6)}$$

where $\Delta = |\Sigma_j J_{ij}\langle \hat{\boldsymbol{J}}_j \rangle|$. We then empirically introduce an intrinsic width for the single-site levels by replacing $\hbar\omega$ with $\hbar\omega + i\Gamma_s$, where the inverse of Γ_s corresponds to the lifetime of the levels. This intrinsic width is necessary to reproduce the broadness of the observed inelastic peak and may most likely be due to scattering of single-site levels by outside perturbations, such as conduction electrons and longer-range interactions, which are not taken into account in the present simple treatment.

The dynamic susceptibilities in the xyz and abn coordinates are related to each other through the following equations:

$$\bar{\bar{\chi}}_i^{0abn}(\hbar\omega) = R_i^{-1}\bar{\bar{\chi}}_i^{0xyz}(\hbar\omega)R_i, \quad \text{(B7)}$$

$$\bar{\bar{\chi}}_{ij}^{abn}(\hbar\omega) = R_i^{-1}\bar{\bar{\chi}}_{ij}^{xyz}(\hbar\omega)R_j. \quad \text{(B8)}$$

Transferred to the above local coordinates, the RPA self-consistent equation (B1) may be solved as

$$\tilde{\chi}^{abn}(\hbar\omega) = \left[\tilde{E} - \frac{1}{2}\tilde{R}\tilde{\chi}^{0abn}(\hbar\omega)\tilde{R}^{-1}\tilde{J}\tilde{R}\right]^{-1}\tilde{\chi}^{0abn}(\hbar\omega), \quad \text{(B9)}$$

where the tilde denotes matrices of the tensors

$$\tilde{\chi}(\hbar\omega) = \begin{pmatrix} \bar{\bar{\chi}}_{11}(\hbar\omega) & \cdots & \bar{\bar{\chi}}_{1N}(\hbar\omega) \\ \vdots & \ddots & \vdots \\ \bar{\bar{\chi}}_{N1}(\hbar\omega) & \cdots & \bar{\bar{\chi}}_{NN}(\hbar\omega) \end{pmatrix}, \quad \text{(B10)}$$

$$\tilde{\chi}^0(\hbar\omega) = \begin{pmatrix} \bar{\bar{\chi}}_1^0(\hbar\omega) & & 0 \\ & \ddots & \\ 0 & & \bar{\bar{\chi}}_N^0(\hbar\omega) \end{pmatrix}, \quad \text{(B11)}$$

$$\tilde{R} = \begin{pmatrix} \bar{\bar{R}}_1 & & 0 \\ & \ddots & \\ 0 & & \bar{\bar{R}}_N \end{pmatrix}, \tag{B12}$$

and J is defined as

$$J = \begin{pmatrix} J_{11} & \cdots & J_{1N} \\ \vdots & \ddots & \vdots \\ J_{N1} & \cdot & J_{NN} \end{pmatrix}, \tag{B13}$$

where N stands for the size of the system—i.e., $N=20$.

For randomly selected 1000 classical ground-state spin configurations, $\tilde{\chi}^{abn}(\hbar\omega)$ is numerically calculated using Eq. (B9) with $J_2=-0.14$ meV and $\Gamma_s=1.8$ meV. (These parameters reproduce experimental results quite well, although they were not refined because the RPA dynamic susceptibility calculation is time consuming.) Then the obtained $\tilde{\chi}^{abn}(\hbar\omega)$ is transferred into xyz coordinates using Eq. (B8) and Fourier transformed using the following equation:

$$\bar{\bar{\chi}}^{xyz}(\boldsymbol{Q},\hbar\omega) = \sum_{ij} \bar{\bar{\chi}}_{ij}^{xyz}(\hbar\omega) e^{-i\boldsymbol{Q}\cdot(\boldsymbol{R}_i-\boldsymbol{R}_j)}, \tag{B14}$$

where $\boldsymbol{R}_i$ ($\boldsymbol{R}_j$) denotes the position of ith (jth) atom. A statistical average was taken for the 1000 numerically obtained dynamic susceptibilities to simulate the frozen state of the Zn-Mg-Tb quasicrystals. We found that the off-diagonal terms in the statistically averaged $\bar{\bar{\chi}}_{ave}^{xyz}(\boldsymbol{Q},\hbar\omega)$ are negligible compared to the diagonal terms. Hence, the trace of $\bar{\bar{\chi}}_{ave}^{xyz}(\boldsymbol{Q},\hbar\omega)$ gives the resulting RPA dynamic susceptibility

$$\chi^{RPA}(\boldsymbol{Q},\hbar\omega) = \sum_{\alpha=x,y,z} \chi_{ave}^{\alpha\alpha}(\boldsymbol{Q},\hbar\omega). \tag{B15}$$

The imaginary part of the resulting RPA dynamic susceptibility is visualized in two manners as described in the text: one is the $\boldsymbol{Q}$-integrated spectrum shown in Fig. 8(a), whereas the other is the $\hbar\omega$-integrated scattering function in the 2F plane, which is shown in Fig. 8(b).

*Electronic address: taku@issp.u-tokyo.ac.jp

[1] D. Shechtman, I. Blech, D. Gratias, and J. W. Cahn, Phys. Rev. Lett. **53**, 1951 (1984).
[2] A. Yamamoto, Acta Crystallogr., Sect. A: Found. Crystallogr. **52**, 509 (1996).
[3] K. Fukamichi, in *Physical Properties of Quasicrystals*, edited by Z. M. Stadnik (Springer-Verlag, Berlin, 1999), pp. 295–326.
[4] E. Y. Vedmedenko, H. P. Oepen, and J. Kirschner, Phys. Rev. Lett. **90**, 137203 (2003).
[5] E. Y. Vedmedenko, U. Grimm, and R. Wiesendanger, Phys. Rev. Lett. **93**, 076407 (2004).
[6] S. Wessel, A. Jagannathan, and S. Haas, Phys. Rev. Lett. **90**, 177205 (2003).
[7] S. Wessel and I. Milat, Phys. Rev. B **71**, 104427 (2005).
[8] A. Niikura, A. P. Tsai, A. Inoue, and T. Matsumoto, Philos. Mag. Lett. **69**, 351 (1994).
[9] I. R. Fisher, K. O. Cheon, A. F. Panchula, P. C. Canfield, M. Chernikov, H. R. Ott, and K. Dennis, Phys. Rev. B **59**, 308 (1999).
[10] H. Takakura, M. Shiono, T. J. Sato, A. Yamamoto, and A. P. Tsai, Phys. Rev. Lett. **86**, 236 (2001).
[11] T. Ishimasa, K. Oyamada, Y. Arichika, E. Nishibori, M. Takata, M. Sakata, and K. Kato, J. Non-Cryst. Solids **334&335**, 167 (2004).
[12] T. Ohno and T. Ishimasa, in *Proceedings of the 6th International Conference on Quasicrystals*, edited by S. Takeuchi and T. Fujiwara (World Scientific, Singapore, 1998), p. 39.
[13] T. J. Sato, H. Takakura, and A. P. Tsai, Jpn. J. Appl. Phys., Part 2 **37**, L663 (1998).
[14] I. R. Fisher, Z. Islam, A. F. Panchula, K. O. Cheon, M. J. Kramer, P. C. Canfield, and A. I. Goldman, Philos. Mag. B **77**, 1601 (1998).
[15] A. Langsdorf and W. Assmus, J. Cryst. Growth **192**, 152 (1998).
[16] Y. Hattori, A. Niikura, A. P. Tsai, A. Inoue, T. Masumoto, K. Fukamichi, H. Aruga-Katori, and T. Goto, J. Phys.: Condens. Matter **7**, 2313 (1995).
[17] T. J. Sato, H. Takakura, A. P. Tsai, K. Shibata, K. Ohoyama, and K. H. Andersen, Phys. Rev. B **61**, 476 (2000).
[18] B. Charrier, B. Ouladdiaf, and D. Schmitt, Phys. Rev. Lett. **78**, 4637 (1997).
[19] Z. Islam, I. R. Fisher, J. Zarestky, P. C. Canfield, C. Stassis, and A. I. Goldman, Phys. Rev. B **57**, R11047 (1998).
[20] T. J. Sato, H. Takakura, A. P. Tsai, and K. Shibata, Phys. Rev. Lett. **81**, 2364 (1998).
[21] T. J. Sato, Acta Crystallogr., Sect. A: Found. Crystallogr. **61**, 39 (2005).
[22] J. Dolinsek, Z. Jaglicic, M. A. Chernikov, I. R. Fisher, and P. C. Canfield, Phys. Rev. B **64**, 224209 (2001).
[23] J. Dolinsek, Z. Jaglicic, T. J. Sato, J. Q. Guo, and A. P. Tsai, J. Phys.: Condens. Matter **15**, 7981 (2003).
[24] M. Scheffer, M. Rouijaa, J. B. Suck, R. Sterzel, and R. E. Lechner, Mater. Sci. Eng., A **294**, 488 (2000).
[25] T. J. Sato, H. Takakura, A. P. Tsai, K. Shibata, K. Ohoyama, and K. H. Andersen (unpublished).
[26] T. J. Sato, H. Takakura, A. P. Tsai, H. Kadowaki, and K. Shibata, J. Phys. Soc. Jpn. Suppl. A, **70**, 224 (2001).
[27] K. Inoue, T. Kanaya, Y. Kiyanagi, K. Shibata, K. Kaji, S. Ikeda, H. Iwasa, and Y. Izumi, Nucl. Instrum. Methods Phys. Res. A **327**, 433 (1993).
[28] K. Inoue, Y. Ishikawa, N. Watanabe, K. Kaji, Y. Kiyanagi, H. Iwasa, and M. Kohgi, Nucl. Instrum. Methods Phys. Res. A **238**, 401 (1985).
[29] S. Ikeda *et al.*, J. Phys. Soc. Jpn. **60**, 3340 (1991).
[30] S. W. Lovesey, *Theory of Neutron Scattering from Condensed Matter* (Oxford University Press, Oxford, 1984), Vol. 2.
[31] A. T. Ogielski, Phys. Rev. B **32**, 7384 (1985).
[32] H. Takayama and H. Yoshino, Physica A **204**, 650 (1994).
[33] A. P. Murani, J. Magn. Magn. Mater. **22**, 271 (1981).
[34] J. Jensen and A. R. Mackintosh, *Rare Earth Magnetism Structure and Excitations* (Clarendon Press, Oxford, 1991).

[35] L. Néel, Ann. Geophys. (C.N.R.S.) **5**, 99 (1949).
[36] B. Frick and D. Richter, Science **267**, 1939 (1995).
[37] T. Kanaya and K. Kaji, Adv. Polym. Sci. **154**, 87 (2001).
[38] U. Buchenau, N. Nucker, and A. J. Dianoux, Phys. Rev. Lett. **53**, 2316 (1984).
[39] D. Kahaner, C. Moler, and S. Nash, *Numerical Methods and Software* (Prentice-Hall, Englewood Cliffs, NJ, 1989).
[40] B. D. Gaulin, J. N. Reimers, T. E. Mason, J. E. Greedan, and Z. Tun, Phys. Rev. Lett. **69**, 3244 (1992).